J Stat Phys (2012) 147:424–435
DOI 10.1007/s10955-012-0474-1

Fractal Iso-Contours of Passive Scalar in Two-Dimensional Smooth Random Flows

Marija Vucelja · Gregory Falkovich · Konstantin S. Turitsyn

Received: 23 November 2011 / Accepted: 24 March 2012 / Published online: 5 April 2012

Abstract A passive scalar field was studied under the action of pumping, diffusion and advection by a 2D smooth flow with Lagrangian chaos. We present theoretical arguments showing that the scalar statistics are not conformally invariant and formulate a new effective semi-analytic algorithm to model scalar turbulence. We then carry out massive numerics of scalar turbulence, focusing on nodal lines. The distribution of contours over sizes and perimeters is shown to depend neither on the flow realization nor on the resolution (diffusion) scale r_d for scales exceeding r_d. The scalar isolines are found to be fractal/smooth at scales larger/smaller than the pumping scale. We characterize the statistics of isoline bending by the driving function of the Löwner map. That function is found to behave like diffusion with diffusivity independent of the resolution yet, most surprisingly, dependent on the velocity realization and time (beyond the time on which the statistics of the scalar is stabilized).

Keywords Mixing fluids · Passive scalar · Statistical geometry · Turbulence

1 Introduction

A fundamental problem in mixing is to describe the iso-contours of the quantity which is mixed (called passive scalar in what follows). This is important for numerous practical applications. Renewed interest in this problem is related to the recent mathematical advances in describing random curves, particularly in identifying an important class of curves SLE_κ

M. Vucelja (✉)
Courant Institute of Mathematical Sciences, New York University, New York, NY 10012-1185, USA
e-mail: vucelja@cims.nyu.edu

G. Falkovich
Department of Physics of Complex Systems, Weizmann Institute of Science, Rehovot, 76100 Israel

K.S. Turitsyn
Department of Mechanical Engineering, Massachusetts Institute of Technology, Cambridge, MA 02139, USA

that can be mapped into a one-dimensional Brownian walk with diffusivity κ. SLE stands for Schramm-Löwner Evolution and presents a fascinating subject where physics meets geometry [9, 21, 25]. If lines belong to an SLE class, as was found in particular for isolines of vorticity and other quantities in turbulent inverse cascades [5, 6, 16], conformal invariance provides exact formulae for the statistical description of the kind unimaginable before in turbulence studies.

Smooth velocity fields $\boldsymbol{v}(\boldsymbol{r})$ are often encountered in nature and industry. Such fields are characterized by an exponential decay of the spectrum $|\boldsymbol{v}_{\boldsymbol{k}}|^2$. For what follows, it is important that the velocity difference between two close points is proportional to the distance, which requires that the mean squared velocity gradient is finite, that is the integral $\int k^2 |\boldsymbol{v}_{\boldsymbol{k}}|^2 d\boldsymbol{k}$ converges at $k \to \infty$. For this it is enough that $|\boldsymbol{v}_{\boldsymbol{k}}|^2$ decays faster than k^{-d-2} and the wavenumber energy spectrum $E(k) \propto k^{d-1} |\boldsymbol{v}_{\boldsymbol{k}}|^2$ decays faster than $\propto k^{-3}$. Examples of spatially smooth yet temporally random flows are: elastic turbulence [22], large-scale turbulence in the Earth's atmosphere (this is a marginal case with approximately $E(k) \propto k^{-3}$ [24]), flows in the phase space of a dynamical system etc.

Mixing in smooth flows is provided by an exponential separation of trajectories and Lagrangian chaos. We consider incompressible fluid flows and Hamiltonian flows in phase space. Generally, such flows have a positive Lyapunov exponent λ so they stretch any element into a long narrow strip. Additionally, our passive scalar is subject to random sources/sinks distributed in space with a correlation scale L. The resulting "passive scalar turbulence" in this (so-called Batchelor [3]) regime has been extensively studied in terms of the one-point probability and multi-point correlation functions [15], one can even write down a closed expression for the probability of any given scalar field realization. Yet to the best of our knowledge, nothing is known about the properties of an infinite-point object, such as an isoline. This may seem surprising since much is known about isolines in a non-smooth (fully turbulent) velocity field [5, 11, 13, 27]. Apparently, the description of contours in the Batchelor regime is more involved. A conceptual difficulty is related to the lack of scale invariance. Indeed, every long contour is simultaneously stretched to the scales far exceeding L and contracted to the scales much less than L in transverse directions. Technically, experimental and numerical studies of passive scalar turbulence in the Batchelor regime are notoriously difficult because of a slow logarithmic dependence of the scalar correlation functions on the resolution [22].

In this work we suggest a new, very effective, method of numerical simulation of passive scalar turbulence in the Batchelor regime. The method is based on the analytic representation of the Lagrangian path integral. We carry out extensive numerical simulations of passive scalar turbulence in two dimensions and find out that the isolines are non-fractal one-dimensional lines at scales less than L. We then show that the isolines are fractal at scales larger than L, and describe the statistics of the contour sizes and perimeters. Finally we explore the relation of these isolines to SLE.

2 Passive Scalar Field

A passive scalar θ is carried by a velocity $\boldsymbol{v}$, forced by φ and diffuses with the molecular diffusivity κ_d:

$$\partial_t \theta + (\boldsymbol{v} \cdot \boldsymbol{\nabla})\theta = \kappa_d \boldsymbol{\nabla}^2 \theta + \varphi. \tag{1}$$

The velocity field $\boldsymbol{v}$ is assumed to be random, incompressible and smooth. We denote the tensor of the local (Lagrangian) velocity gradients as $\sigma_{ij} \equiv \partial v_i / \partial r_j$. The statistics of the

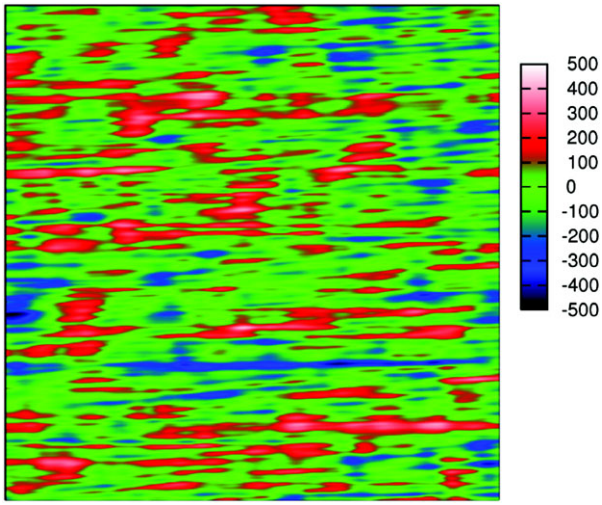

Fig. 1 A snapshot of the passive scalar field of size $(75L)^2$ (L is the forcing scale). The *color bar* shows the magnitude of the scalar field (Color figure online)

velocity and its gradients is white in time and spatially isotropic:

$$\left\langle \sigma_{ij}(t)\sigma_{kl}\left(t'\right)\right\rangle = \lambda[3\delta_{ik}\delta_{jl} - \delta_{ij}\delta_{kl} - \delta_{il}\delta_{jk}]\delta\left(t-t'\right) = \nabla_i\nabla_k K_{jl}\delta\left(t-t'\right), \tag{2}$$

where K_{jl} is the velocity correlation function. The pumping $\varphi(t,\boldsymbol{r})$ is assumed to be a random field with correlation radius L. It is believed that the statistics of the scalar field is independent of the details of the temporal statistics of $\varphi(t,\boldsymbol{r})$ as long as it has a finite correlation time. In what follows we consider $\varphi(t,\boldsymbol{r})$ to be either (i) a Poisson process of independently adding size-L blobs of passive scalar at random positions and with random amplitudes, see Sect. 3, or (ii) white Gaussian with zero mean and variance $\overline{\varphi(t,\boldsymbol{r})\varphi(0,\boldsymbol{0})} = \delta(t)\chi(|\boldsymbol{r}|)$, where $\chi(|\boldsymbol{r}|)$ decays faster than any power at $|\boldsymbol{r}| > L$, see Sect. 4.

3 The New Computational Method

Previously, passive scalar turbulence was simulated by a pseudo-spectral code (see e.g. [12, 19, 20] and references in [15]). In such simulations the numerical Fourier transform limits the maximal attainable resolution of the scalar field. In the Batchelor regime, the caveat is that the spatial resolution already has to be very large to compute the pair correlation function of θ, which has a slow logarithmic decay [15]. In contrast to pseudo-spectral codes, the method we use is spatially local, since it does not involve taking a numerical Fourier transform. Our method is based on treating the flow and the pumping separately: we solve the flow evolution exactly and model the pumping by adding blobs of scalar given by (3) below. The scalar dynamics is pre-computed for every single blob of scalar obeying Eq. (1) with $\varphi = 0$. A snapshot of the scalar field $\theta(t,\boldsymbol{r})$ is then obtained as a sum over blobs, generated at random positions and random times in the past, that have independently evolved in time (see Fig. 1). Here we exploit the linearity of the advection-diffusion equation (1) and the smoothness of the velocity field. We assume that each blob at its initial time t_0 had an isotropic shape centered around a random position $\boldsymbol{r}_{0C}$ and having a random amplitude Θ_0:

$$\theta(t_0,\boldsymbol{r}_0) = \Theta_0 \exp\left[-(\boldsymbol{r}_0 - \boldsymbol{r}_{0C})^2/\left(2L^2\right)\right]. \tag{3}$$

The (elliptical) shape of such a blob at a later time t is found by the method of characteristics. In this method a PDE is rewritten as an ODE along a characteristic (i.e. a fluid trajectory). We first pass to the reference frame of a fluid element $\theta(t,\boldsymbol{r}) = \theta(t, \boldsymbol{y} + \boldsymbol{R}(\boldsymbol{r}_{0C}, t_0; t)) \equiv \vartheta(t, \boldsymbol{y})$, here $\boldsymbol{y}$ is the coordinate in the local frame and $\boldsymbol{R}(\boldsymbol{r}_{0C}, t_0; t)$ is the Lagrangian trajectory that obeys $\boldsymbol{R}(\boldsymbol{r}_{0C}, t_0; t_0) = \boldsymbol{r}_{0C}$. The advection-diffusion equation in the co-moving frame reads

$$\partial_t \vartheta(t,\boldsymbol{y}) + y_j \sigma_{ij} \frac{\partial \vartheta(t,\boldsymbol{y})}{\partial y_i} = \kappa_d \nabla_{\boldsymbol{y}}^2 \vartheta(t,\boldsymbol{y}). \tag{4}$$

Next we Fourier transform Eq. (4) and then apply the method of characteristics. The ODE that the Fourier transform of ϑ, labeled as $\hat{\vartheta}$, obeys is $\frac{d\hat{\vartheta}[s,\boldsymbol{k}(s)]}{ds} + \kappa_d \boldsymbol{k}^2(s)\hat{\vartheta}[s,\boldsymbol{k}(s)] = 0$, where $\boldsymbol{k}(s) = (W(s,t_0)^T)^{-1}\boldsymbol{k}(t_0)$ is the wavenumber along the characteristic and $W(t,t_0)$ is the evolution operator, defined as: $\boldsymbol{R}(\boldsymbol{r}_0, t_0; t) = W(t,t_0)\boldsymbol{r}_0$. The solution of this ODE is

$$\hat{\vartheta}\big[t,\boldsymbol{k}(t)\big] = \hat{\vartheta}\big[t_0, W(t,t_0)^T\boldsymbol{k}(t)\big] \exp\left[-\frac{1}{2}\boldsymbol{k}(t)^T Q(t,t_0)\boldsymbol{k}(t)\right], \tag{5}$$

where $Q(t,t_0) \equiv 2\kappa_d \int_{t_0}^{t} (W(t,t_0)W(t',t_0)^{-1})(W(t,t_0)W(t',t_0)^{-1})^T dt'$ and $\hat{\vartheta}[t_0, W(t,t_0)^T \cdot \boldsymbol{k}(t)] = (2\pi)L^2\Theta_0 e^{-\frac{1}{2}(W(t,t_0)^T\boldsymbol{k}(t))^T W(t,t_0)^T\boldsymbol{k}(t)L^2}$ is the Fourier transform of the blob at time t_0 (see Eq. (3)). Thus the Fourier transform of the blob at time t is

$$\hat{\vartheta}\big[t,\boldsymbol{k}(t)\big] = (2\pi)L^2\Theta_0 e^{-\frac{1}{2}\boldsymbol{k}(t)^T I(t,t_0)\boldsymbol{k}(t)}, \tag{6}$$

where we denote $I(t,t_0) \equiv W(t,t_0)W(t,t_0)^T L^2 + Q(t,t_0)$. This quantity is actually the tensor of inertia of a blob $I = (1/N)\int d\boldsymbol{r} r_\alpha r_\beta \theta$, where $N \equiv \int d\boldsymbol{r}\theta$ is an invariant of Eq. (4). It is easy to see since both definitions satisfy the same differential equation $\partial_t I + \sigma I + I\sigma^T + 2\kappa_d = 0$. Fourier transforming Eq. (6) and changing to the fixed reference frame yields the shape of the blob at time t

$$\theta(t,\boldsymbol{r}) = \frac{\Theta_0 L^2}{\sqrt{\det I(t,t_0)}} e^{-\frac{1}{2}[\boldsymbol{r}-W(t,t_0)\boldsymbol{r}_{0C}]I^{-1}(t,t_0)[\boldsymbol{r}-W(t,t_0)\boldsymbol{r}_{0C}]}. \tag{7}$$

Note that there are seven values that specify a blob at time t: the symmetric matrix $I(t,t_0)$, Θ_0, $\boldsymbol{r}_c(t) \equiv W(t,t_0)\boldsymbol{r}_{0C}$ and t_0.

Forcing statistics. The amplitudes of the blobs, Θ_0, are i.i.d. variables, with a normal distribution, of zero mean and variance $\langle\Theta_0^2\rangle = 100$. Blob "births" are modeled as a homogeneous Poisson process with rate parameter ν. Thus ν is the expected number of "blob births" that occur per unit time at a given point in space. Empirically we have found that approximately 4.5×10^3 blobs intersect at each pixel of our image, i.e. each pixel is sum of that many i.i.d. variables. The Central Limit Theorem asserts that as n gets larger, the distribution of a sum of n i.i.d. variables approaches a Gaussian distribution (see e.g. [17]). One can estimate the deviations from the limiting normal distribution via the generalized Berry-Esseen theorem [7, 14, 18], which gives an upper bound of $\mathcal{O}(n^{-1/2})$. In our simulations, we thus estimate that the forcing differed from a Gaussian by $\mathcal{O}(10^{-3/2})$. A scalar field with forcing and dissipation is statistically stable for times $T_s \propto \lambda^{-1}\ln(L/r_d) \sim O(1)$. Our runs were much longer than T_s (the simulations had $T\lambda \in \{20, 50, 100\}$, where $r_d/L \in \{0.06, 0.03, 0.015\}$, which amounts to $T_s \leq 4$).

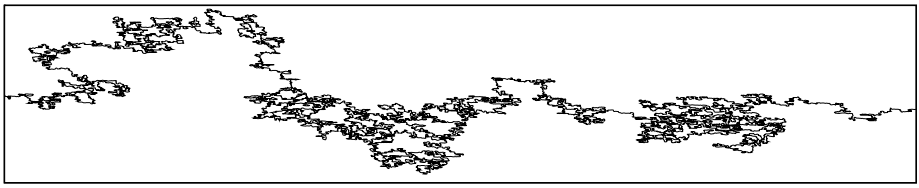

Fig. 2 A long scalar iso-contour in a window of $2400L \times 360L$, where L is the forcing scale

Velocity statistics. We modeled the velocity gradient matrix σ as: $\sigma_{11} = a$, $\sigma_{12} = b + c$, $\sigma_{21} = b - c$ and $\sigma_{22} = -a$, were a, b and c are Gaussian variables with zero mean and variance $\langle a(t)a(t')\rangle = \langle b(t)b(t')\rangle = \langle c(t)c(t')\rangle/2 = \lambda\delta(t - t')$. This gives us a velocity field that is incompressible ($\mathrm{tr}(\sigma) = 0$) and whose stress and strain are approximately equal in magnitude ($\langle \det\sigma \rangle = 0$). Numerically the correlation time of σ was one time step ($\Delta t = 0.01\lambda$).

Methods to analyze the nodal lines of the scalar. We identify the individual contours of an iso-set of θ by MATLAB's *contourc* function. This built-in function uses linear interpolation to parametrize the isoline by points that sit on the edges of the discretized θ field. Its error is smaller than $(r_d/L)^2 \max\{|\nabla_i \nabla_j \theta|\}\frac{1}{8}$, where (r_d/L) is the distance between two neighboring passive scalar data points and $\max\{|\nabla_i \nabla_j \theta|\}$ is the maximal second order derivative of θ between two neighboring points. In our simulations typically $\max\{|\nabla_i \nabla_j \theta|\}\frac{1}{8} = \mathcal{O}(1)$, which amounts to an interpolation error of the order of $(r_d/L)^2$. An example of a long contour can be seen in Fig. 2. On the isolines, we measure the box-counting generalized fractal dimensions: $D_q \equiv \lim_{\varepsilon\to 0} \log(\sum_i^{N(\varepsilon)} p_i^q(\varepsilon))[(q-1)\log(\varepsilon)]^{-1}$. Here $p_i(\varepsilon)$ is the probability of finding a point in the i-th square of area ε^2, and $N(\varepsilon)$ is the number of ε^2 squares needed to cover the contour. For long contours, we study the statistics of bending by making the Löwner map of the half-plane minus curve into a half-plane [5, 23]. As one goes along the curve, the image moves along the half-plane boundary; if this motion (called driving function) is Brownian then the curve belongs to SLE class.

4 Theoretical Expectations

At times exceeding the pumping correlation time, the pumping alone would produce a Gaussian field θ whose zero isolines are smooth at the scales below L, while at larger scales the isolines are those of critical percolation (class of curves called SLE_6 and having dimension $D_0 = 7/4$). The velocity field by itself does not change the statistics of θ as it just rearranges it; the flow stretches isolines uniformly in the direction of the eigenvector of the positive Lyapunov exponent and contracts transversal to it. Nontrivial statistics of θ and its isolines arises from an interplay of velocity, pumping and finite diffusivity or finite resolution, which leads to the dissipation of θ and reconnection of isolines that come closer than the resolution scale r_d. We assume $r_d \ll L$. At the scales between L and r_d, there is a cascade of the passive scalar whose correlation functions are logarithmic: $\langle \theta^n(\mathbf{0})\theta^n(\boldsymbol{r})\rangle \sim \ln^n(L/r)$ [3]. Lower orders, $n < \ln(L/r)$, correspond to a Gaussian probability density function (PDF), while the PDF tails are exponential [15]. The scalar field itself is thus non-smooth at $r < L$, what about its isolines? If the scalar were a Gaussian (free) field with logarithmic correlation functions, it would have isolines with fractal dimension 3/2. However the Gaussian

probability functional,

$$\mathcal{P}\{\theta\} \propto \exp\left[-\frac{\mu}{2}\int d\boldsymbol{r}\left|\nabla\theta(\boldsymbol{r})\right|^2/\chi(\boldsymbol{0})\right], \tag{8}$$

does not satisfy the Fokker-Planck equation, which can be derived for the scalar field under the action of both velocity and pumping, which are white in time:

$$\frac{\partial\mathcal{P}}{\partial t} = \frac{1}{2}\iint d\boldsymbol{r}_1 d\boldsymbol{r}_2 \frac{\delta^2}{\delta\theta(\boldsymbol{r}_1)\delta\theta(\boldsymbol{r}_2)}\big[K_{\alpha\beta}\nabla_\alpha\theta(\boldsymbol{r}_1)\nabla_\beta\theta(\boldsymbol{r}_2) - \chi\big(|\boldsymbol{r}_1-\boldsymbol{r}_2|\big)\big]\mathcal{P} + \kappa_d\int d\boldsymbol{r}_1\frac{\delta}{\delta\theta(\boldsymbol{r}_1)}\nabla^2\theta(\boldsymbol{r}_1)\mathcal{P}. \tag{9}$$

By substituting (8) in (9) we see that already the first term gives a non-vanishing contribution:

$$\iint d\boldsymbol{r}_1 d\boldsymbol{r}_2 \lambda\mathcal{P}\big\{2\big[\nabla\theta(\boldsymbol{r}_1)\cdot\nabla\theta(\boldsymbol{r}_2)\big]^2 - \left|\nabla\theta(\boldsymbol{r}_1)\right|^2\left|\nabla\theta(\boldsymbol{r}_2)\right|^2\big\}. \tag{10}$$

Since it is the highest order in θ, it cannot be canceled by any other terms so that the Fokker-Planck equation is not satisfied and the statistics is non-Gaussian. Indeed, we know that correlation functions of θ include cumulants [1]. One may argue that the cumulants contain less logarithmic factors than reducible terms and are small [15]. However, the properties of the isolines must depend on those cumulants, since they contribute to the correlation functions of the gradients at the leading order.

Likewise it is straightforward to establish that the correlation functions of the passive scalar are not conformally invariant, i.e., for instance, the four-point function does not have the form

$$F_4 = f\left(\frac{r_{12}r_{34}}{r_{13}r_{24}}, \frac{r_{12}r_{34}}{r_{14}r_{23}}\right)(r_{12}r_{34}r_{14}r_{23}r_{13}r_{24})^a. \tag{11}$$

Indeed, we know from [1] that $F_4 = F(\boldsymbol{r}_{12},\boldsymbol{r}_{34}) + F(\boldsymbol{r}_{13},\boldsymbol{r}_{24}) + F(\boldsymbol{r}_{14},\boldsymbol{r}_{23})$. This is compatible with (11) only for $F(x,y) = (xy)^{a/2} + (xy^{-2})^{a/2} + (x^{-2}y)^{a/2}$ which leads to $F_4 = (r_{12}r_{34})^{2a} + (r_{13}r_{24})^{2a} + (r_{14}r_{23})^{2a}$, i.e. to a Gaussian statistics. However we have just shown (see previous paragraph) that θ differs from a Gaussian free field. Therefore, passive scalar is not in any way close to a free field and its statistics is not conformally invariant.

If one tries to find an analogy with a non-Gaussian field having logarithmic correlation functions, such as the height function built from independently oriented loops in the $O(n)$ model [10], the deviations of $|\kappa-4|$ and $|D-3/2|$ are proportional to cumulants in this case. Another much exploited similarity is between the passive scalar and the vorticity cascade of two-dimensional turbulence; vorticity was shown to have multifractal isolines with dimensionalities changing from 3/2 to 1 [6].

5 Numerical Results and Discussion

Let us now confront theoretical expectations with the results of numerics. We made several velocity realizations with different resolutions $r_d/L \in \{0.06, 0.03, 0.015\}$, pumping frequencies $\nu/\lambda \in \{0.2, 0.5, 1, 2\}$ and scalar evolution times $T\lambda \in \{20, 50, 100\}$.

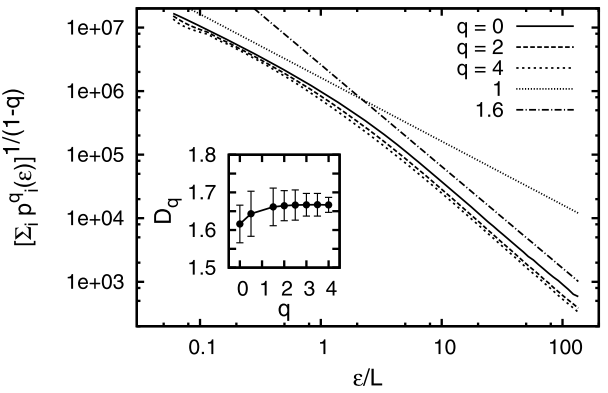

Fig. 3 The generalized box counting fractal dimension D_q is scale dependent. Below the forcing scale L the curves are smooth with $D_q = 1$, while above L, the contour seems to be a simple fractal with D_q in between 1.55–1.7. The pumping frequency was $\nu/\lambda = 1$

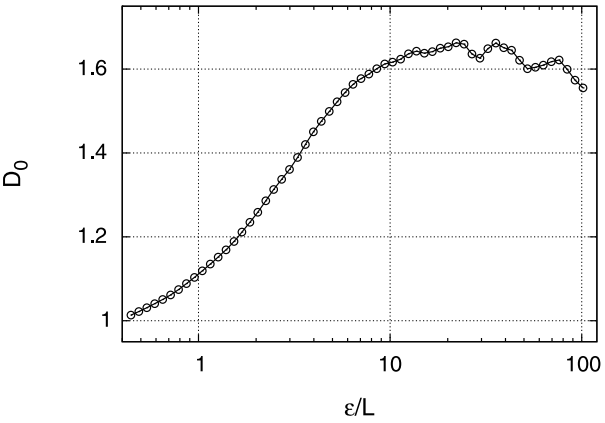

Fig. 4 The box counting fractal dimension D_0, for $\nu/\lambda = 1$, estimated from the slope: $d \log N(\varepsilon)/d \log(L/\varepsilon)$. It is scale dependent and we see that bellow the forcing scale L the curves are smooth with $D_0 = 1$, while above L, the contour seems to be a fractal having D_0 in the range 1.55–1.7

5.1 Fractal Dimension

Despite all of the suggestive similarities, presented in the previous section, we see that scalar isolines are smooth below L. Figures 3 and 4 show the box-counting dimensions of contours. Actually the fact that the scalar isolines are smooth below L is quite natural from the physical perspective since all of the factors (velocity, pumping, diffusion) are smooth at these scales. In particular, that means that the scalar field non-smoothness is related to the discontinuities of θ across (smooth) isolines. Within our accuracy, we cannot see any difference between the dimensions of the different orders and conclude that our contours are mono-fractals, which is distinct from the multi-fractal iso-vorticity contours in a direct cascade of $2d$ turbulence [5]. This difference might be due to the fact that all parts of our scalar contours go through the same history of velocity, while parts of a long vorticity contour may have different histories.

5.2 The Statistics of Contour Sizes and Perimeters

Let us now describe the probability density function (PDF) of contour perimeters P and sizes characterized by the mean radius $R \equiv \sqrt{\langle(\boldsymbol{\rho} - \langle\boldsymbol{\rho}\rangle)^2\rangle}$, here $\boldsymbol{\rho}$ denotes the pairs of points parameterizing a contour and averaging $\langle\cdot\rangle$ is done over the points. Figures 5 and 6 present the PDFs of $\log(P/L)$ and $\log(R/L)$ and show that they depend neither on the resolution

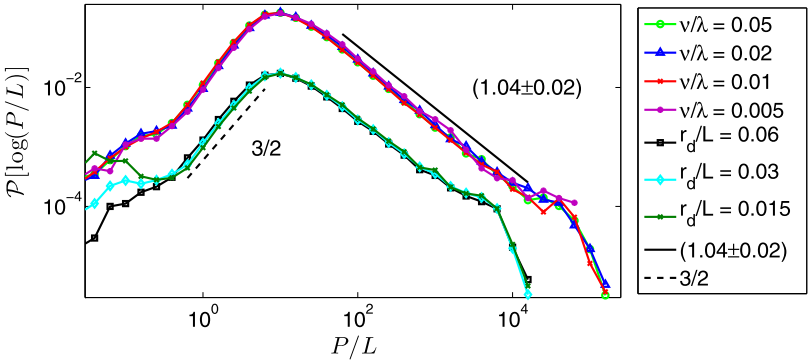

Fig. 5 The PDF of perimeters for different pumping frequencies (*upper three curves*) and resolutions (*lower three curves*). *Lower three* are shifted down by dividing by 10, without shifting all curves collapse together (Color figure online)

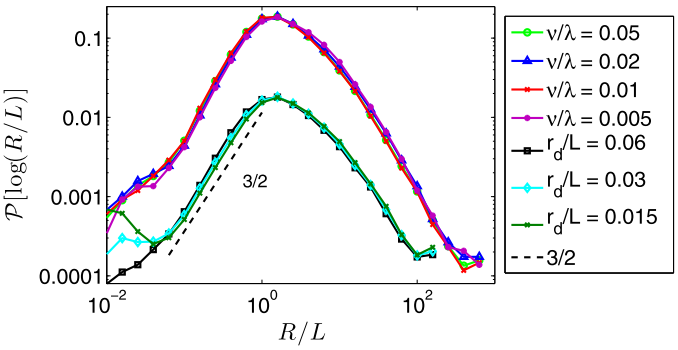

Fig. 6 The PDF of sizes for different pumping frequencies (*upper three curves*) and resolutions (*lower three curves*). *Lower three* are shifted down by dividing by 10, without shifting all curves collapse together (Color figure online)

for $r_d/L = 0.015$–0.06 nor on the pumping frequency for $\nu/\lambda = 0.2$–2. In both figures, the upper three curves are at different ν/λ and have the same $r_d/L = 0.06$; while the lower three curves (PDF of those was divided by 10) differ in r_d/L and have the same $\nu/\lambda = 1$. Lower three are shifted down only for visualization purposes, without shifting all curves collapse together.

Let us consider separately the left and right tails of the PDFs. Since the probability of contours much larger than r_d is independent of diffusion then it must be determined by an interplay of stretching and pumping. Figures 5 and 6 show that the left tails of both $\mathcal{P}(P)$ and $\mathcal{P}(R)$ look like a power law with the power $3/2$. Contours shorter than L must appear when pumping cuts a piece off a long thin contour, the probability of such a cut is $\propto P \propto R$ (small contours are smooth so that $P \propto R$). The extra factor $\sqrt{P} \propto \sqrt{R}$ in the PDF may appear because, to be observed, small contours need to survive without being swallowed by further pumping events, the lifetime is likely to be $\propto \sqrt{P} \propto \sqrt{R}$. Since creation and survival are independent events, their probabilities are multiplied.

What should one expect for the PDFs of contour sizes at scales exceeding L? It is tempting to assume that a long contour appears due to an evolution undisturbed by pump-

Table 1 Generalized fractal dimensions, for different pumping frequencies ν/λ

ν/λ	D_0	D_2	D_4
0.2	1.61 ± 0.05	1.66 ± 0.02	1.67 ± 0.02
0.5	1.62 ± 0.03	1.65 ± 0.05	1.65 ± 0.05
1	1.62 ± 0.05	1.67 ± 0.05	1.67 ± 0.03
2	1.62 ± 0.03	1.68 ± 0.06	1.68 ± 0.04

ing during a long time t. The length of such a contour is $L\exp(\lambda t)$ as long as it does not exceed L^2/r_d. The probability that the pumping did not act during the time t is given by a Poisson law $\exp(-\nu t)$ where ν is the pumping correlation time (in our algorithm, an average time between producing blobs of θ in a given place). We then obtain $\mathcal{P}(R) = \int dt \exp(-\nu t)\delta(R - \exp(\lambda t)) \propto R^{-1-\nu/\lambda}$, which would mean that the PDF tail is non-universal and depends on the statistics of pumping and velocity. If that was true, one would expect the same tail for the PDF of perimeters as well. However, the above consideration totally disregards the fractal nature of long contours (shown in Fig. 3). We have checked that the fractal dimensions within our error bars were the same for different pumping frequencies ν, see Table 1. In line with long contour fractality, the right tails of the PDFs of P and R are very different. The tail of the PDF of sizes, $\mathcal{P}(R)$, looks log-normal, see Fig. 6. The tail of $\mathcal{P}(P)$ looks like a universal power law, independent of the resolution and the pumping frequency ν, see Fig. 5. In log coordinates the tail is close to $1/P$ so it may be that $\mathcal{P}(P) \propto P^{-2}$, yet we were unable to derive this law theoretically so far.

Looking at Figs. 5 and 6, a natural question is whether the positions of the maxima depend on the resolution. Pumping produces more or less circular contours of radius L, which are then deformed into ellipsoids of increasing eccentricity by the velocity field. Pumping continues to act by bending elongated contours. Those contours that on average have not changed much by this bending disappear after reaching the length of order L^2/r_d and respectively the width of order the coarse-graining scale r_d. One then asks if the scale L^2/r_d is special, apart from L and r_d. Numerics gives a negative answer: lower curves in Figs. 5 and 6 compare runs with three different r_d and show that the PDFs do not depend on the resolution for the scales exceeding r_d. In particular, the PDFs of the sizes have the maximum at the pumping scale L independently of the resolution (or diffusion scale). We checked that the statistics is practically the same for either an average distance of the contour points from their center of mass or the maximal distance between the points of the contour (gyration radius). The PDFs of perimeter also have maxima independent of the diffusion scale (at the size approximately $2\pi L$). The only difference one can distinguish in the lower curves in Figs. 5 and 6 is the appearance of the secondary maximum at small scales for the curve with the best resolution, there the resolution scale $0.015L$ is comparable with the diffusion scale, which is $0.01L$ in all runs; in other words, there is an abundance of diffusion-scale contours.

5.3 Löwner Map Characterization of Curves

Quite unusual statistics of the passive scalar lacking scale-invariance has been found at $r > L$: multi-point correlation functions strongly depend on geometry [2]. This is because of the highly anisotropic "strip" structure of the field seen clearly in Fig. 1. Let us discuss the statistics of bending for the isolines extending for such long distances. If there was only pumping then on the scales larger than L the scalar would be a short-correlated field whose nodal lines are equivalent to critical percolation, i.e. SLE_6. Without diffusion and with infinite resolution, velocity only distorts the field. Of course, distorted field is not SLE

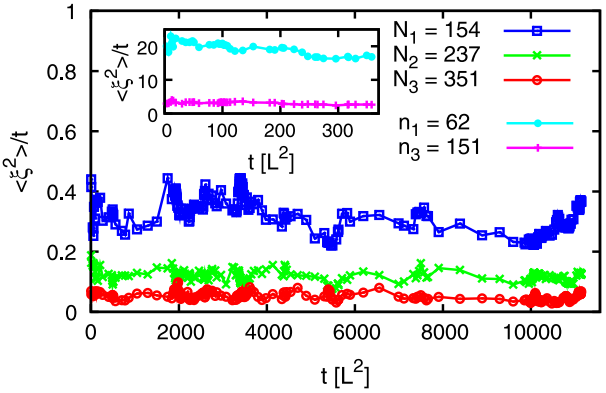

Fig. 7 Effective diffusivity of the driving function $\xi(t)$ for different velocity realizations (1–3), where t is time in Löwner's equation, see [25]. The curves are ensemble averages of N_i contours (*inset*: of n_i contours) from the i-th velocity realization. *Inset* shows the effective diffusivity for velocity realizations 1 and 3 after contraction by L/r_d. The pumping frequency was $\nu/\lambda = 1$ (Color figure online)

[23]; for instance, stretching vertically a chordal SLE in a half-plane one adds to the driving function extra intervals of no change, that diminishes κ and provides for a finite correlation scale (equivalently, finite correlations in Löwner time t which is the coordinate along the contour). And yet, deforming it back with a time-dependent distortion factor $\exp(2\lambda T)$, we would get the same SLE_6. While the restoration procedure itself may be not very practical since real flows consist of many such domains oriented randomly, the very possibility of it means potential availability of very useful exact formulae describing the statistics of contours. For example, one may be able to describe crossing and surrounding probabilities (like Cardy-Smirnov formula [8, 26]) with just a simple re-scaling. However, a finite resolution/diffusion leads to irreversible changes. Indeed, when velocity distorts the contours, it causes some distances in the contracting directions to become less than the resolution scale r_d which leads to reconnections and disappearance of thin contours. Now it is highly nontrivial if any trace of initial SLE can be recovered, and if yes, after what contraction. One may try to estimate the stretching factor empirically by measuring the aspect ratio of the boxes one can fit the contours into; we found out that this approach does not work since such an aspect ratio fluctuates strongly (by several orders of magnitude).

Let us recall that Oseledec theorem and a general theory of Lagrangian chaos with diffusion [15] state that any finite-point statistic is independent of the velocity realization and can be understood under the assumption that the effective contraction factor is L/r_d. This is based on the fact that Lyapunov exponents are self-averaging and the mean lifetime of scalar blobs is $\lambda^{-1}\ln(L/r_d)$. If one is to extend this reasoning to the statistics of an infinite-point object, then one expects the isoline statistics to depend strongly on the resolution scale r_d and be independent of the velocity realization in a steady state and for sufficiently long contours that appear after a long history of stretching. As we now see, both predictions fail spectacularly.

As was already stated above, we characterize the behavior of a single line by the driving function of the Löwner map. Figure 7 shows that driving functions behave roughly as that of diffusion and so can be characterized by the diffusivity $\kappa = \langle \xi^2(t)\rangle/t$. As seen in Fig. 8, the diffusivity is independent of the resolution scale (this may be related to the problem of noise sensitivity in the statistics of random curves [4]). It is also independent of the contour sizes as long as they are larger than L, yet κ is different in different velocity realizations even on the same very long Löwner timescale (i.e. for very long contours). Most dramatically, Fig. 8 shows that κ depends strongly on the time T of stretching. That dependence continues on extremely long timescales far exceeding the time $\lambda^{-1}\ln(L/r_d)$ during which the scalar field itself acquires stationary statistics. We conclude that long contours undergo stretching and

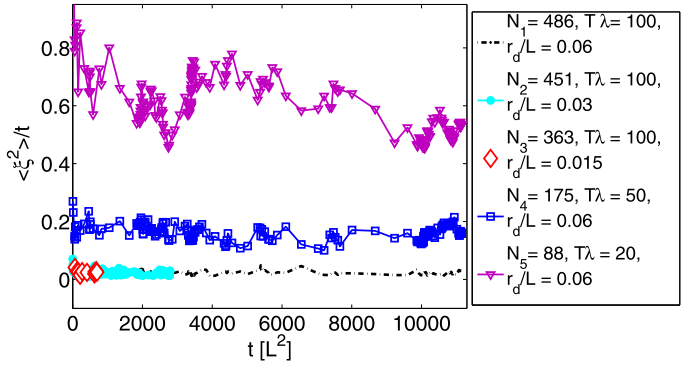

Fig. 8 Effective diffusivity of the driving function $\xi(t)$ for different resolution scales and the evolution times $T\lambda$ for the same velocity realization. N_i show the number of contours we averaged over and label the curves. Graphs N_1, N_2 and N_5 show that $\kappa = \langle \xi^2(t) \rangle / t$ depends on the evolution time $T\lambda \in \{20, 50, 100\}$, while N_1, N_2 and N_3 show that κ does not depend on the resolution $r_d/L \in \{0.015, 0.03, 0.06\}$. The curves of different resolutions are of different length since the time of the Löwner map is measured in the units of length squared and for a better resolution we used a smaller physical window (all scalar snapshots had 40000^2 pixels, but in terms of the forcing scale they had $(600L)^2$, $(1200L)^2$, $(2400L)^2$ respectively). The pumping frequency was $\nu/\lambda = 1$ (Color figure online)

their statistics changes on a much larger timescale than the scalar blob lifetime. Let us stress the discrepancy: κ depends strongly on the distortion and yet it is independent of r_d (at least within the limits we studied), that is the effective distortion factor for long isolines is not L/r_d (as it is for multi-point statistics). On the other hand, note that choosing the contraction factor equal to L/r_d one obtains κ of the "right" order of magnitude (between 3 and 17 for different velocity realizations, see inset of Fig. 7). One is tempted to explore whether one can recover SLE contours (despite all the loss of information due to reconnections) by fine-tuning the distortion factor, possibly by requiring either restoration of statistical isotropy or shortest correlation time of $\xi(t)$. Further studies with extensive statistics are needed to sort out which properties of the critical percolation are retained by the large-scale statistics of passive scalar contours in the Batchelor regime.

Acknowledgements This research was supported by the NSF grant PHY05-51164 at KITP, and by the grants of BSF, ISF and Minerva foundation at the Weizmann Institute. We benefited from discussions with I. Binder, G. Boffetta, D. Dolgopyat, A. Celani, K. Khanin, J.P. Eckmann, S. Smirnov and C. Connaughton.

References

1. Balkovsky, E., Chertkov, M., Kolokolov, I., Lebedev, V.: Fourth-order correlation function of a randomly advected passive scalar. JETP Lett. **61**, 1012 (1995)
2. Balkovsky, E., et al.: Large-scale properties of passive scalar advection. Phys. Fluids **11**, 2269–2279 (1999)
3. Batchelor, G.K.: Small-scale variation of convected quantities like temperature in turbulent fluid. Part 1. General discussion and the case of small conductivity. J. Fluid Mech. **5**, 113–133 (1959)
4. Benjamini, I., Kalai, G., Schramm, O.: Noise sensitivity of Boolean functions and applications to percolation. Publ. Math. IHES **90**, 5–43 (1999)
5. Bernard, D., et al.: Conformal invariance in two-dimensional turbulence. Nat. Phys. **2**(2), 124–128 (2006)
6. Bernard, D., et al.: Inverse turbulent cascades and conformally invariant curves. Phys. Rev. Lett. **98**(2), 024501 (2007). doi:10.1103/PhysRevLett.98.024501

7. Berry, A.C.: The accuracy of the Gaussian approximation to the sum of independent variates. Trans. Am. Math. Soc. **41**, 122–136 (1941)
8. Cardy, J.: Critical percolation in finite geometries. J. Phys. A **25**, 201–206 (1992)
9. Cardy, J.: SLE for theoretical physicists. Ann. Phys. **318**, 81–118 (2005)
10. Cardy, J., Ziff, R.: Exact results for the universal area distribution of clusters in percolation, Ising, and Potts models. J. Stat. Phys. **110**, 1 (2003)
11. Catrakis, H.J., Dimotakis, P.E.: Scale distributions and fractal dimensions in turbulence. Phys. Rev. Lett. **77**(18), 3795–3798 (1996)
12. Celani, A., Lanotte, A., Mazzino, A., Vergassola, M.: Universality and saturation of intermittency in passive scalar turbulence. Phys. Rev. Lett. **84**, 2385–2388 (2000)
13. Constantin, P.: Geometric statistics in turbulence. SIAM Rev. **36**(1), 73–98 (1994)
14. Esseen, C.G.: On the Liapunoff limit of error in the theory of probability. Arkiv Mat. Astron. Fysk. **28**, 1–19 (1942)
15. Falkovich, G., Gawedzki, K., Vergassola, M.: Particles and fields in fluid turbulence. Rev. Mod. Phys. **73**, 913–975 (2001)
16. Falkovich, G., Musacchio, S.: Conformal invariance in inverse turbulent cascades. arXiv:1012.3868
17. Feller, W.: An Introduction to Probability Theory and Its Applications, vol. 1, 3rd edn. Wiley, New York (1968)
18. Feller, W.: On the Berry–Esseen theorem. Probab. Theory Relat. Fields **10**, 261–268 (1968)
19. Fereday, D.R., Haynes, P.H.: Scalar decay in two-dimensional chaotic advection and Batchelor-regime turbulence. Phys. Fluids **16**(12), 4359–4370 (2004)
20. Gotoh, T., Nagaki, J., Kaneda, Y.: Passive scalar spectrum in the viscous-convective range in two-dimensional steady turbulence. Phys. Fluids **12**(1), 155–168 (2000)
21. Gruzberg, I.A., Kadanoff, L.P.: The Loewner evolution: maps and shapes. J. Stat. Phys. **30**, 8459–8469 (2004)
22. Jun, Y., Steinberg, V.: Mixing of passive tracers in the decay Batchelor regime of a channel flow. Phys. Fluids **22**, 123101 (2010)
23. Kennedy, T.: Computing the Loewner driving process of random curves in the half plane. J. Stat. Phys. **131**, 803–819 (2008)
24. Nastrom, G., Gage, K.: The kinetic energy spectrum of large- and mesoscale atmospheric processes. Tellus, Ser. A **35**, 383–386 (1983)
25. Schramm, O.: Scaling limits of loop-erased random walks and uniform spanning trees. Isr. J. Math. **118**, 221–288 (2000)
26. Smirnov, S.: Critical percolation in the plane: conformal invariance, Cardy's formula, scaling limits. C.R. Acad. Sci. I Math. **333**, 239–244 (2001)
27. Sreenivasan, K.R.: On local isotropy of passive scalars in turbulent shear flows. Proc. R. Soc. Lond. A **434**, 165–182 (1991)